

Runway Wake Vortex, Crosswind, and Visibility Detection with a Scintillometer at Schiphol Airport



CrossMark

ARTICLE

Runway Wake Vortex, Crosswind, and Visibility Detection with a Scintillometer at Schiphol Airport

D. van Dinther 1 · O. K. Hartogensis 1 · A. A. M. Holtslag 1

Received: 29 September 2014 / Accepted: 14 July 2015 / Published online: 1 September 2015 © The Author(s) 2015. This article is published with open access at Springerlink.com

Abstract We evaluate the performance and investigate the capability of a scintillometer to detect wake vortices, crosswind and visibility near an airport runway. An experiment is carried out at Schiphol airport (Amsterdam, The Netherlands), where an optical scintillometer is positioned alongside a runway. An algorithm is developed to detect wake vortices, and also the strength of the wake vortex, from the variance in the scintillation signal. The algorithm shows promising results in detecting wake vortices and their strengths during the night. During the day, the scintillometer signal is dominated by environmental turbulence and wake vortices are no longer detectable. The crosswind measured by the scintillometer is compared with wind-speed and wind-direction data at the airport. Our results show that, after applying an outlier filter, the scintillometer is able to measure the crosswind over the short time period of 3 s required for aviation applications. The outlier filter does not compromise the capability of the scintillometer to obtain the maximum 3 s crosswind over a 10-min time frame correctly. Finally, a transmission method is used to obtain the visibility from the scintillometer signal, which is then compared with that obtained from a visibility sensor. The scintillometer is able to identify periods of low visibility correctly, although it shows a high amount of scatter around the exact visibility value.

 $\textbf{Keywords} \quad \text{Airport} \cdot \text{Crosswind} \cdot \text{Scintillometry} \cdot \text{Transverse wind} \cdot \text{Visibility} \cdot \\ \text{Wake vortices}$

1 Introduction

The safety of aircraft landing and taking off is dependent on critical weather and environmental conditions. Examples are strong crosswinds, tailwind events, thick fog, rainfall and wake vortices created by other aircraft. To minimise the risk of accidents, aircraft operations

Meteorology and Air Quality Group, Wageningen University, Wageningen, The Netherlands



 [○] O. K. Hartogensis oscar.hartogensis@wur.nl

are limited to certain weather conditions. Most weather conditions are monitored by point measurements, which can be affected by local conditions or ground clutter close by. Therefore, such measurements may not be representative of the meteorological conditions on the runway. In this study, we present a line-averaged measurement technique using an optical scintillometer to detect wake vortices, crosswind and visibility near an airport runway.

A scintillometer consists of a transmitter and receiver, typically spaced a few hundred metres to a few kilometres apart. The transmitter emits light at a specific wavelength, which is refracted by the turbulent eddy field in the atmosphere, resulting in light intensity fluctuations at the receiver. The more turbulent the atmosphere, the more vigorous the intensity of the fluctuations in the scintillometer signal. These fluctuations are linked to surface fluxes, since heat exchange causes more turbulence in the atmosphere. Obtaining path-averaged surface fluxes has been the main application of scintillometers to date (e.g. Meijninger and de Bruin 2000; Green et al. 2001).

Here, we investigate the applicability of a scintillometer to detect wake vortices. The lift of the wings of aircraft creates wake vortices, which can pose safety issues for following aircraft landing or taking off. Therefore, there are strict rules concerning the separation between two aircraft landing or taking off (Gerz et al. 2002). However, these rules limit airport capacity. A monitoring system for wake vortices can help to ensure airport safety and increase airport capacity. Various studies (e.g. Harris et al. 2002; Gerz et al. 2005; Holzäpfel and Steen 2007) focus on Doppler lidar measurements to detect wake vortices. However, Doppler lidars have problems with retrieving the correct wind speed and wind direction near the surface. The reason is that the return signal of the ground also influences the signal (Godwin et al. 2012). Hallock and Osgood (2003) showed that wake vortices can also be obtained from a large array of sonic anemometers (in the study of Hallock and Osgood (2003) a sonic every 50 m). A scintillometer with one transmitter and one receiver should suffice to detect wake vortices along the touch-down or take-off zone.

Different studies (e.g. Lawrence et al. 1972; Wang et al. 1981; Poggio et al. 2000) have already shown that a scintillometer is able to obtain the crosswind correctly. The crosswind (U_{\perp}) is the wind component perpendicular to a path. Most of the validation studies for a scintillometer measuring U_{\perp} have taken place over flat grassland sites (e.g. Poggio et al. 2000; van Dinther et al. 2013; van Dinther and Hartogensis 2014), over which U_{\perp} can be assumed constant along the scintillometer path. Around airport runways, the scintillometer signal will be affected by turbulence induced by aircraft, however. We will therefore investigate whether the algorithms to obtain U_{\perp} from scintillometer measurements are still applicable near airport runways. We test if U_{\perp} can be obtained from a scintillometer over the 3-s time scale used in aviation, while previous studies used time scales in the order of 10s (van Dinther and Hartogensis 2014).

Fog at airports causes delays and thereby limits airport capacity (e.g. Robinson 1989; van der Velde et al. 2010). Nowadays, fog at airports is in general measured by point measurements (e.g. transmissometer). We investigate the ability of a scintillometer to obtain a path-averaged value for the visibility. Fog results in a lowering of the scintillation signal, since the water droplets in fog scatter light, so that the light transmitted by the transmitter is not captured by the receiver (Earnshaw et al. 1978). Potentially, the drop in the scintillometer signal can be linked to the visibility.

Thus, the goal of this study is to investigate the feasibility and performance of a scintillometer to detect wake vortices, crosswind and visibility. The investigation is carried out based on scintillometer data collected in the summer of 2013 near a busy runway at Schiphol airport in Amsterdam, The Netherlands.



2 Theory

The receiver of a scintillometer measures light intensity fluctuations caused by the turbulent atmosphere through which the light travels. The turbulent eddy field in between the transmitter and receiver is constantly changing due to eddy decay and transport by the wind for the scintillometer type used here. A scintillometer measures over very short time scales (measurement frequency of 500 Hz), which makes Taylor's frozen turbulence hypothesis applicable (i.e. the eddy field does not change while it is transported through the scintillometer path). The only driver of changes in the eddy field is therefore the wind. Given the path length of scintillometers (a few hundred metres to a few kilometres), the sole driver is actually the crosswind (U_{\perp}). More information on scintillometry can be found, e.g., in Andreas (1990), De Bruin (2002) and Wheelon (2006). The background theory of the three subjects investigated (wake vortices, crosswind and visibility) is briefly described in the following sections.

2.1 Wake Vortices

The lift force exerted on an aircraft wing creates wake vortices, as follows: First, a strong downward motion develops behind the trailing edge of the wing, while a weaker upward motion develops behind the wing tips (Gerz et al. 2002). Therefore, small spiraling motions develop at the wing tips and landing flap. Through a phenomenon known as roll-up, these small motions develop into the wake vortex with single- and double-branched spirals (Krasny 1987). The strength of the circulation of a wake vortex is proportional to the weight of the aircraft and the order of the wing span (Gerz et al. 2002).

Wake vortices deform and weaken, and thereby decay under the influence of secondary vorticity structures (Holzäpfel et al. 2003). There are multiple quantities that influence the lifetime and trajectory path of wake vortices, such as ambient wind, turbulence, wind shear and turbulence stratification (Gerz et al. 2005). Besides these quantities, near the ground, wake vortices can separate and rebound, leading to their decay (Robins and Delisit 1993). Robins and Delisit (1993) found that, under stable conditions, wake vortices are able to survive up to 3.5 min and travel perpendicular under the influence of the crosswind. Unfortunately, they did not state information about the lifetime of wake vortices near the ground for unstable conditions. The long lifetime under stable conditions allows wake vortices to be transported from one runway to a neighbouring runway. Thus, a wake vortex detection system is crucial for airport safety.

2.2 Crosswind

Different methods exist to obtain scintillometer-based U_{\perp} , relying either on scintillation spectra or the time-lagged correlation function $(r_{12}(\tau))$. Scintillation spectra can be obtained from a single-aperture scintillometer, while $r_{12}(\tau)$ must be obtained from a dual-aperture scintillometer (i.e. two spatially separated scintillometers). The benefit of $r_{12}(\tau)$ is that it can be obtained over shorter time scales than scintillation spectra (10s compared with 10 min) (van Dinther and Hartogensis 2014). Furthermore, from $r_{12}(\tau)$, the sign of U_{\perp} (i.e. the side from which the flow is directed into the scintillometer path) can also be obtained. For the application at airports, U_{\perp} needs to be obtained over a short time scale (3s), which is necessary to determine the wind gust and wind lull. Therefore, we rely on a method which uses $r_{12}(\tau)$.



The values of $r_{12}(\tau)$ are obtained from a dual-aperture scintillometer by shifting one of the two signals in time and calculating the correlation between the two signals. In theory, the two signals should be identical at a certain time lag, since the eddy field does not change while it is being transported from one scintillometer to the other. The higher the U_{\perp} value, the shorter the time lag between the two signals.

Lawrence et al. (1972) developed a theoretical model for the time-lagged covariance function ($C_{12}(\tau)$), based on earlier work of Tatarskii (1961). Including the aperture averaging terms of a large-aperture scintillometer (Wang et al. 1981), the theoretical model of Lawrence et al. (1972) reads

$$C_{12}(\tau) = 16\pi^{2}k^{2} \int_{0}^{1} \int_{0}^{\infty} K\phi_{n}(K) \sin^{2}\left[\frac{K^{2}Lx(1-x)}{2k}\right] J_{0}\{K[s(x) - U_{\perp}(x)\tau]\}$$

$$\left[\frac{2J_{1}(0.5KD_{R}x)}{0.5KD_{R}x}\right]^{2} \left\{\frac{2J_{1}[0.5KD_{T}(1-x)]}{0.5KD_{T}(1-x)}\right\}^{2} dKdx, \tag{1}$$

where k is the wavenumber of the emitted radiation, K is the turbulent spatial wavenumber, $\phi_n(K)$ is the three-dimensional spectrum of the refractive index in the inertial range given by Kolmogorov (1941), L is the scintillometer path length, x is the relative location on the path, J_0 is the zero-order Bessel function, s(x) is the separation distance between the two beams at location x along the path, τ is the time lag, J_1 is the first-order Bessel function, D_R is the aperture diameter of the receiver, and D_T is the aperture diameter of the transmitter. From Eq. 1, the theoretical variance (C_{11}) can also be calculated, by taking s(x) = 0 and $\tau = 0$. The theoretical $r_{12}(\tau)$ can be obtained by dividing the theoretical $C_{12}(\tau)$ by the theoretical C_{11} . Here, we assume that $C_{11} = C_{22}$, which is the case when D_R and D_T are the same for the two scintillometers.

2.3 Visibility

A variety of visibility sensors exist, relying on different methods to obtain the visibility. The most classical is the transmission method, where a transmitter and receiver are aligned over a certain path. The receiver measures the amount of light left after the transmitted light has travelled along the path. Other methods rely on forward- and back-scattering to measure the visibility. A scintillometer uses the transmission method, since the transmitter and receiver are aligned directly across from one another.

Visibility measurement devices in general use the Lambert–Beer law, which for a scintillometer reads

$$I_{\rm R} = I_{\rm T} e^{-aL},\tag{2}$$

where I_R is the light intensity measured by the receiver of the scintillometer, I_T is the light intensity emitted by the transmitter, and a is the attenuation coefficient. The coefficient a is a measure of the amount of attenuation due to absorption and scattering of the light in the atmosphere (Vogt 1968). This absorption or scattering can be caused by different effects, e.g. dust, water droplets and aerosols.

To ensure a detectable signal over the range of the scintillometer measurement path (for a large-aperture scintillometer, typically $500-5000\,\mathrm{m}$), either I_R (i.e. the sensitivity of the receiver to measure the light intensity) or I_T of the scintillometer can be adjusted. For the scintillometer used in this study (BLS900; Scintec, Rottenburg, Germany), I_R is adjusted through discrete attenuation settings in order to ensure a suitable level of I_R for scintillometer measurements.



Koschmieder (1924) was the first to link visibility (V) to a, by stating that, during daylight conditions, 2 % of light had to be detected by a receiver in order for a human eye to detect an object. In other words, I_R/I_T , also known as the transmission factor (T), is 0.02. Applying the relation L = V for T = 0.02 to Eq. 2 gives

$$V = \frac{-\ln 0.02}{a}.$$
 (3)

The meteorological optical range (MOR) is a quantity often used in aviation to describe the visibility. According to Werner et al. (2005), MOR is defined as the limit at which at least 5 % of the light is received, i.e.

$$MOR = \frac{-\ln 0.05}{a} \approx \frac{3}{a},\tag{4}$$

which gives the relation between MOR and a. Substituting a into Eq. 2, we obtain the expression for MOR

$$MOR = \frac{L \ln 0.05}{\ln \left(I_R / I_T \right)},\tag{5}$$

so that MOR is expressed in terms of the scintillometer emitted light, I_T , and the measured quantity I_R .

3 Methods

3.1 Wake Vortex Detection

Wake vortices create extra turbulence around an airport runway, and thus leave a trace in the scintillation signal, making it potentially possible to determine them using a scintillometer. The variance of the log of the light intensity measured by the receiver $(\sigma_{\ln I}^2)$ can be interpreted as the amount of turbulence in the atmosphere. Hence, the extra turbulence created by a wake vortex should lead to an increase in $\sigma_{\ln I}^2$. In order to determine if a wake vortex is present, the value of $\sigma_{\ln I}^2$ is compared with the running median $\sigma_{\ln I}^2$ of the previous 5 min $(\sigma_{\ln I}^2)$. Thereby, we assume that the value of $\sigma_{\ln I}^2$ is an approximate value of the amount of background turbulence in the atmosphere. The algorithm we developed to detect a wake vortex consists of the following criteria:

$$-\frac{\sigma_{\ln I}^2}{\sigma_{\ln I}^2} > 1.8 \times \overrightarrow{\sigma_{\ln I}^2}$$
$$-\frac{\sigma_{\ln I}^2}{\sigma_{\ln I}^2} < 2 \times 10^{-4}$$

- $-I_{\rm R} > \frac{2}{3}$ of the maximum $I_{\rm R}$ $(I_{\rm R,max})$
- At least ten consecutive points have to meet the criteria above

The criteria stated above can in principle be applied to different scintillometer set-ups, except for the second criterion ($\sigma_{\ln I}^2$ < 2 × 10⁻⁴). This criterion is applied since the scintillometer is unable to detect wake vortices in an unstable atmosphere (as will be shown in Sect. 5.1). The value of $\sigma_{\ln I}^2$ of 2 × 10⁻⁴ corresponds to a value of the structure parameter of the refractive index (C_{n^2}) of 9 × 10⁻¹⁵ m^{-2/3}. The value of C_{n^2} is in principle applicable for any scintillometer set-up.

For detection of wake vortices, the criteria given above worked well (as will be shown in Sect. 5.1). However, to determine the length of a wake vortex, the criterion of $\sigma_{\ln I}^2 > 1.8 \times$



 $\overrightarrow{\sigma_{\ln I}^2}$ appeared to be too strict. Therefore, for determining the length of the wake vortex, a less strict filter of $\sigma_{\ln I}^2 > 1.2 \times \overrightarrow{\sigma_{\ln I}^2}$ is applied, which should also be applicable for any scintillometer set-up.

Besides detecting if a wake vortex is present, we also develop an algorithm to determine the strength of a wake vortex (S_{WV}) . The strength is determined from the magnitude of $\sigma_{\ln I}^2$; the stronger the wake vortex, the more turbulence the wake vortex generates, and the higher $\sigma_{\ln I}^2$. The value of S_{WV} is therefore determined by the 95 % percentile of $\sigma_{\ln I}^2$ during the wake vortex normalised by the $\overline{\sigma_{\ln I}^2}$ just before the wake vortex, resulting in a S_{WV} of arbitrary units.

No other measurement devices were recording wake vortices at the time of the experiment, which made it impossible to directly validate the wake vortices detected by the scintillometer with independent measurements. However, the Air Traffic Control The Netherlands (LVNL) keeps track of when and on which runway an aircraft is landing or taking off. All aircraft have a wake turbulence category given by the International Civil Aviation Organization, which is either "light", "medium", "heavy" or "super", based on the weight and other specifications of the aircraft. These wake turbulence category specifications together with the airport's operations (landing or take off) were available from day of the year (DOY) 184 until 221 in 2013. Note that, during this time period, only aircraft with a wake turbulence category of medium and heavy landed or took off from the runway at which the scintillometer was measuring. The time at which aircraft land and take off, together with the wake turbulence category, can be used to validate the wake vortex strength and timing retrieved from the scintillation signal. In order for a detected wake vortex to be attributed to an aircraft, the time between the landing or taking off and the detected wake vortex has to be less than 3.5 min, following the maximum lifetime of a wake vortex reported by Robins and Delisit (1993).

From the aircraft operations we can also calculate how many wake vortices of aircraft can in principle be detected by the scintillometer. This is achieved by using similar criteria as mentioned above to detect wake vortices, but for one minute averages from before the aircraft landed or took off; the average $\sigma_{\ln I}^2$ had to be below 2×10^{-4} , while the average I_R had to be I_R 0 had to be I_R 1. The wake vortex detection results of the scintillometer are given in Sect. 5.1.

3.2 Crosswind

The crosswind is calculated from the scintillometer signal by using the look-up table method described in van Dinther and Hartogensis (2014). This method compares the time-lagged correlation function $(r_{12}(\tau))$ measured by a dual-aperture scintillometer to that of a look-up table. The values of $r_{12}(\tau)$ of the look-up table are calculated using the theoretical model of Lawrence et al. (1972). The U_{\perp} value of the theoretical $r_{12}(\tau)$ that is most similar to the measured $r_{12}(\tau)$ is the U_{\perp} value representative for the time period. More details on the look-up table method are given in van Dinther and Hartogensis (2014). The look-up table method has been proven to work over a flat grassland site. However, it is unclear whether this method is also applicable near airport runways where turbulence created by aircraft also influences the scintillation signal.

The time window over which $r_{12}(\tau)$ is determined should be 10 s (van Dinther and Hartogensis 2014). However, as mentioned above, for aviation a time window of 3 s is necessary. In this study, U_{\perp} was thus determined over a 3-s time window. In order to minimise the effect of not determining $r_{12}(\tau)$ over a sufficient time window, an outlier detection filter is applied. Note that, in practice, for aviation only a filter that makes use of the data taken before a sample can be applied. From the U_{\perp} measurements, a running median is calculated over a period of



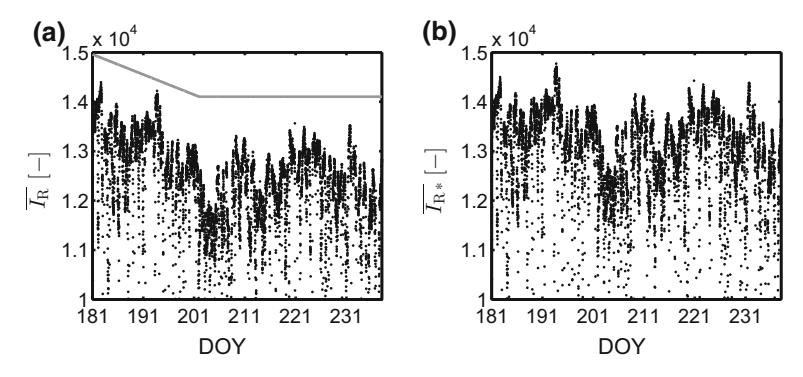


Fig. 1 a Average scintillometer signal over $10 \min (\overline{I_R})$ from day of the year (DOY) 181 until 241 in *black dots* zoomed into the higher values $(\overline{I_R} \ge 1.0 \times 10^4)$, with the line (*grey solid line*) with which $\overline{I_R}$ was adjusted. **b** Normalised 10-min averaged scintillometer signal $(\overline{I_{R*}})$ after adjusting for alignment issues from DOY 181 until 241 zoomed into the higher values $(\overline{I_{R*}}) \ge 1.0 \times 10^4$)

5 min. If the value of U_{\perp} is 2.5 m s⁻¹ more than the running median, U_{\perp} is classified as an outlier and is not taken into account for further analysis.

3.3 Visibility

In order to measure visibility, defined as MOR, using a scintillometer, the Lambert–Beer law (Eq. 5) is used, which is valid during daylight conditions. In order to determine MOR, I_R and I_T must be determined. The value of I_R is variable and measured by the scintillometer. The value of I_T is constant and for this scintillometer unknown, and thus needs to be determined from the measurements. We calibrate I_T using MOR measurements from a Vaisala FD12P sensor. This calibration is valid for this type of scintillometer, given the attenuation setting used in this study (see Sect. 4.1). Note that only daylight hours are considered during this study, thus measurements in between 2000 and 0500 UTC are excluded from the visibility analysis.

In order to measure MOR with a scintillometer, we assume that I_R is only influenced by the visibility and not by other issues (e.g. misalignment, dirty lenses). However, in Fig. 1a, it can be seen that at the beginning of the experiment the 10-min averaged I_R ($\overline{I_R}$) decreases. This decrease appears to be in no way related to the visibility (not shown here), and therefore it must be caused by alignment issues. Therefore, $\overline{I_R}$ is corrected by dividing it by the values of the grey solid line in Fig. 1a and then multiplying by 1.5×10^4 , resulting in an adjusted 10-min averaged scintillometer signal ($\overline{I_{R*}}$) given in Fig. 1b.

4 Experimental Set-Up and Data Treatment

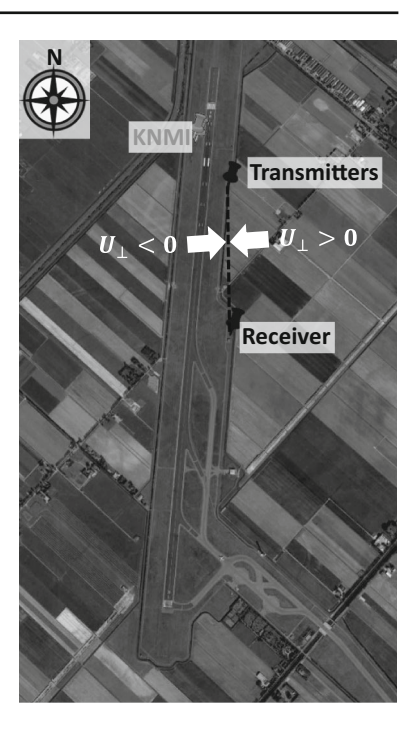
Section 4.1 specifies the experimental set-up used in this study. In order to be able to compare the crosswind measured by the scintillometer with those collected by the Royal Netherlands Meteorological Institute (KNMI), additional data treatment had to be applied. Details on the data treatment are specified in Sect. 4.2.

4.1 Set-Up

The data were collected at Schiphol airport in The Netherlands on the so-called Polderbaan runway from 26 July until 29 August 2013. The runway has approximately a north–south



Fig. 2 Experimental set-up at Schiphol airport with the transmitters and receiver of the scintillometer indicated in *black*; the wind and visibility measurements of KNMI are given in *grey*



orientation (see Fig. 2). In this study the crosswind is defined as positive if, when looking from the transmitters to the receiver, the wind is blowing from the left into the scintillometer path. For this north–south set-up, the crosswind is positive when the wind blows from the east.

The transmitters and receiver of a BLS900 scintillometer (Scintec AG, Rottenburg, Germany) measured over a 1060-m path at height of 3.2 m with geographical orientation of 177° N (see Fig. 2). Given this path length, the attenuation setting of the scintillometer was set to values appropriate for a path ranging from 750 to 1500 m. The transmitters of the BLS900 emit near-infrared light with wavelength of 880 nm. The scintillometer was installed approximately 150 m from the runway. The measurement frequency of the BLS900 was 500 Hz, from which the raw data were saved.

The data of the scintillometer are compared with data collected by KNMI, including wind and visibility data at Schiphol. The wind data were collected by a cup anemometer and wind vane at height of $10 \,\mathrm{m}$ (see Fig. 2), and contain the horizontal wind speed (U) and the wind direction (WD).

The anemometer has a measurement frequency of 4 Hz, from which the 3-s running mean data sample (U_{Sample}) is saved every 12 s, as well as the maximum 3-s sample over the last 12 s, average over the last 10 min (\overline{U}), maximum over the last 10 min ($Max_{U\perp}$), minimum over the last 10 min and standard deviation of the 3-s U values over the last 10 min (STD_U).

The wind vane measures the wind direction every $0.25 \, \mathrm{s}$. The maximum change in wind direction between two samples is allowed to be 8.44° . Greater differences are probably due to errors in the measurement. Just like U, the values of WD are saved every $12 \, \mathrm{s}$. These are as follows: average WD over the last $12 \, \mathrm{s}$, vectorial mean over the last $10 \, \mathrm{min}$, waximum veering wind over the last $10 \, \mathrm{min}$, minimum



backing wind over the last 10 min and standard deviation of the 12-s WD over the last 10 min $(STD_{WD}).$

The value of MOR is measured by KNMI with a Vaisala FD12P sensor at height of about 2.5 m every minute. This sensor uses the forward scattering method, and emits light at an angle of 33°. The transmitter emits infrared light with wavelength of 875 nm. The following quantities are saved: average over the last 1 min, average over the last 10 min (\overline{MOR}) , maximum over the last 10 min, minimum over the last 10 min and standard deviation of the 12-s MOR values over the last 10 min.

4.2 Data Treatment

The horizontal wind-speed data of KNMI are corrected when the wind speed is greater then a certain threshold ($U_{\text{Threshold}}$). It is assumed that wind speeds above $U_{\text{Threshold}}$ are caused by wake vortices of aircraft. $U_{\text{Threshold}}$ is given by Meulen (1998) as

$$U_{\text{Threshold}} = \overline{U} + C_1 ST D_U + 0.5, \tag{6}$$

where C_1 is a constant equal to 4. When $U_{\text{Sample}} > U_{\text{Threshold}}$, the horizontal wind speed can be corrected (U_{Cor}) using (Meulen 1998)

$$U_{\text{Cor}} = \overline{U} + C_2 ST D_U + 0.5, \tag{7}$$

where C_2 is a constant equal to 2. However, Eq. 7 can only be applied if the following criteria are met:

- $-STD_U > 0.5 \,\mathrm{m \, s^{-1}}$ $-\overline{U} > 0.5 \,\mathrm{m \, s^{-1}}$
- $-U_{\rm Sample} < 15 \, {\rm m \, s^{-1}}$
- At least 90% of the data are available

If the criteria above are not met, U_{Sample} is not saved. Note that only the corrected horizontal wind speed is saved, making it impossible to verify the detected wake vortices of the scintillometer with the anemometer measurements.

The scintillometer measured at a height of 3.2 m, while the wind data collected by KNMI are measured at a height of 10 m. Therefore, a logarithmic wind profile was used to transpose U_{\perp} measured by the scintillometer at a height of 3.2 m to 10 m. For simplicity, we used a neutral wind profile, thereby ignoring the effect of stability. Applying the neutral wind profile gives

$$U(10) = \frac{U(3.2)}{\ln\left(\frac{3.2}{z_0}\right)} \ln\left(\frac{10}{z_0}\right),\tag{8}$$

where U(10) and U(3.2) are the wind speed at height of 10 and 3.2 m, respectively, and z_0 is the roughness length (z_0) . In this study, z_0 was assumed to be 0.03 m on the flat grassland side. By applying Eq. 8 for U_{\perp} , we assume that the wind direction does not change with height. Note that the outlier filter specified in Sect. 3.2 is applied before transposing U_{\perp} measured by the scintillometer to a height of 10 m.

An important parameter for aviation is the 10-min maximum in U_{\perp} (Max $_{U\perp}$). However, Max_{U+} is not saved by KNMI, but only the maximum 10-min horizontal wind speed. In this study, the value of $\text{Max}_{U\perp}$ is thus calculated from Max_U and WD. However, given a variable wind direction during the 10-min time interval, the value of $Max_{U\perp}$ may be unrepresentative. Therefore, $Max_{U\perp}$ was excluded from the data analysis when $STD_{WD} > 20^{\circ}$.



5 Results and Discussion

5.1 Wake Vortex Detection

In this section, the results of the wake vortex detection algorithm specified in Sect. 3.1 are discussed. First, two examples of the performance of the algorithm in stable and unstable conditions are given. Second, we show the wind fields under which aircraft were landing and taking off during the studied period. Third, the number of detected wake vortices and number of landings and take offs are discussed. Last, we look at the wake vortex strength, wake vortex size and separation time between an aircraft movement and the detected wake vortex.

Figure 3a shows the wake vortices detected by the scintillometer on DOY 186 between 0330 and 0350 UTC. For this time period there is a clear increase in $\sigma_{\ln I}^2$ after an aircraft landed. The wind direction and crosswind speed over the shown time period transport the wake vortices to the scintillometer path given the experimental setup of this study (see Sect. 4.1). Thus, we can assume that the increase in $\sigma_{\ln I}^2$ is caused by a wake vortex. However, a wake vortex is not detected for all the aircraft that landed; For example, the aircraft with a wake turbulence category of heavy landing at 033437 UTC does not lead to a wake vortex detection. The increase of $\sigma_{\ln I}^2$ after the aircraft landed is only small (with a maximum of 1.4×10^{-4} compared with a $\sigma_{\ln I}^2$ of 6.4×10^{-5}), and only a few points show an elevated $\sigma_{\ln I}^2$ (6, albeit not consecutive). Thereby, the detection criteria stated in Sect. 3.1 are not met. It is possible

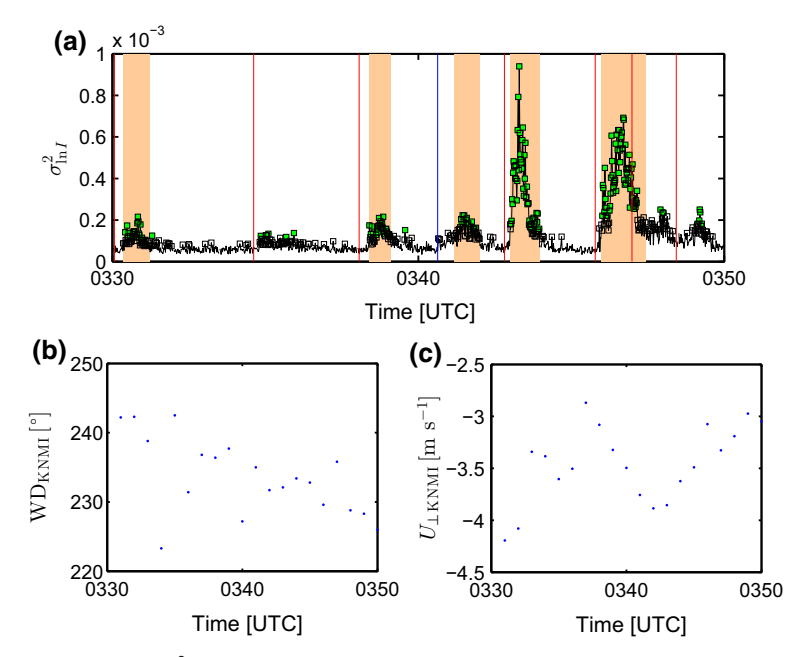


Fig. 3 a Time series of $\sigma_{\ln I}^2$ measured by the scintillometer on DOY 186 between 0330 and 0350 UTC. The *solid lines* indicate when an aircraft was landing (*blue* for an aircraft with wake turbulence category of medium, and *red* for an aircraft with wake turbulence category of heavy). The *green dots* indicate when $\sigma_{\ln I}^2$ is high to indicate a wake vortex. The *black squares* indicate until when a wake vortex is taken into account. The *orange shaded areas* indicate the time period over which the algorithm specified in Sect. 3.1 finds a wake vortex. **b** Wind direction and **c** crosswind measured by KNMI over the same time period (1-min average)



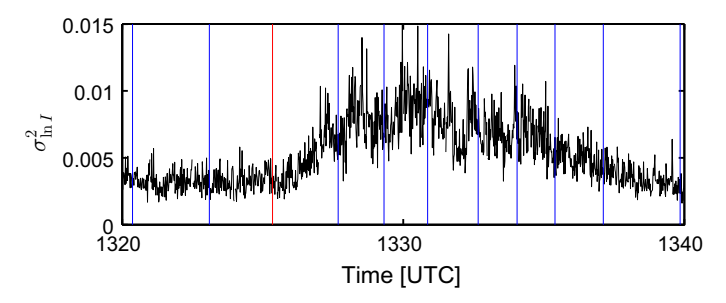


Fig. 4 Time series of $\sigma_{\ln I}^2$ measured by the scintillometer on DOY 184 between 1320 and 1340 UTC. The solid lines indicate when an aircraft was landing (blue for an aircraft with wake turbulence category of medium, and red for an aircraft with wake turbulence category of heavy)

that the wake vortex had already decayed before reaching the scintillometer path, or that it was transported away from the scintillometer path (with a wind direction of 223° at the time). Note that other factors such as the exact place of landing/taking off and plane morphology can also affect the decay and detectability of wake vortices. Figure 3 shows a typical example of the detectability of wake vortices during the night. In the end, we can conclude that, for these nighttime stable conditions, the scintillometer is, in general, able to detect when a wake vortex is present.

Figure 4 shows $\sigma_{\ln I}^2$ for similar wind conditions as Fig. 3 (not shown here, but $220^\circ \le WD \le 250^\circ$ and $-5 \,\mathrm{m\,s^{-1}} \le U_\perp \le -2.5 \,\mathrm{m\,s^{-1}}$), during daytime conditions. For these conditions, the influence of the wake vortices on the scintillation signal is not visible. Apparently, during the day the scintillometer signal is dominated by the background atmospheric turbulence, making it impossible to detect wake vortices from $\sigma_{\ln I}^2$. To ensure that there are no false detections of wake vortices due to the background atmospheric turbulence, the criterion of $\overline{\sigma_{\ln I}^2} < 2 \times 10^{-4}$ is included in the detection algorithm (see Sect. 3.1). Implicitly this criterion is a stability filter; the lower $\overline{\sigma_{\ln I}^2}$, the more stable the atmosphere.

Before looking into the number of wake vortices detected by the scintillometer, we first investigate the wind direction and speed under which landings and take offs occur (Fig. 5a, b). Note that, in this figure, only aircraft for which the wake vortices can potentially be detected (using the criteria stated in Sect. 3.1) are taken into account. There is a clear difference in wind directions under which landings and take offs occur, since aircraft need to keep their nose into the wind. Landings mainly take place for wind directions of 180–270°, while take offs take place for wind directions of 350–60°. The wind speed is in general greater for aircraft landing (typically 6–7 m s⁻¹) than taking off (typically 4–5 m s⁻¹). Given the scintillometer set-up in this experiment (see Sect. 4.1), the landings should be more easily detectable, since the wake vortices are transported towards the scintillometer path.

The wind roses of the wake vortices detected by the scintillometer are shown in Fig. 5c, d. The wake vortices created by aircraft landing are detected for wind directions of $220-230^{\circ}$, while the wake vortices created by aircraft under wind directions of $180-220^{\circ}$ are not detected. This implies that the wake vortices are indeed transported by the wind. For aircraft taking off the wake vortices are mainly detected when the wind speed is relatively weak ($\leq 4 \,\mathrm{m \, s^{-1}}$). The wake vortices created by aircraft taking off under the influence of strong wind speed would be transported away from the scintillometer path. There are also some (in total 39) wake vortices detected when there was no aircraft landing or taking off within the previous $3.5 \,\mathrm{min}$, which we refer to as false detections. The wind rose of these false detections is



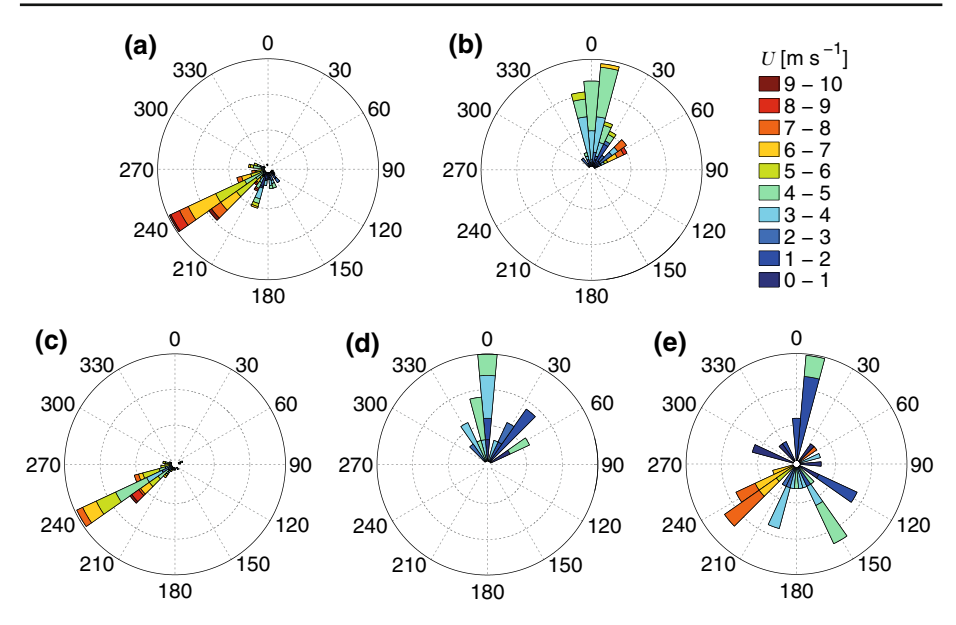


Fig. 5 Wind roses of aircraft **a** landing and **b** taking off in conditions where the wake vortices are detectable by the scintillometer, coloured according to the horizontal wind speed. Wind roses of the detected wake vortices for aircraft **c** landing, **d** taking off and **e** false detections, coloured according to the horizontal wind speed

Table 1 Number of aircraft for which the wake vortices can potentially be detected by the scintillometer, together with the number of wake vortices (landing, take off and false) detected by the scintillometer given the corresponding wake turbulence category of the aircraft

	U_{\perp}	Landing			Take off			False
		Medium	Heavy	Total	Medium	Heavy	Total	
Aircraft	> 0	35	6	41	92	12	104	
Aircraft	< 0	161	52	213	25	3	28	
Detected	> 0	4	0	4	9	4	13	20
Detected	< 0	71	44	115	7	0	7	19

plotted in Fig. 5e. The false detections seem to occur for random wind directions and wind speed.

Table 1 states the number of wake vortices detected by the scintillometer, as well as the number of wake vortices that are potentially detectable using the criteria stated in Sect. 3.1. Note that we do not expect that all the wake vortices created by aircraft will be detected, since some wake vortices can decay before reaching the scintillometer path or not reach the scintillometer path at all due to transport by wind. From the total of 386 potentially detectable wake vortices, 139 wake vortices were detected. There were also 39 false detections, which occur due to other phenomena that influence the scintillometer signal, such as background atmospheric turbulence, insects and dust. As expected, the scintillometer detects more wake vortices created by aircraft landing than taking off (63 % compared with 15 % of the total potentially detectable), which is highly likely to be caused by the wind directions under which each process occurs (Fig. 5). The influence of transport of wake vortices by wind is



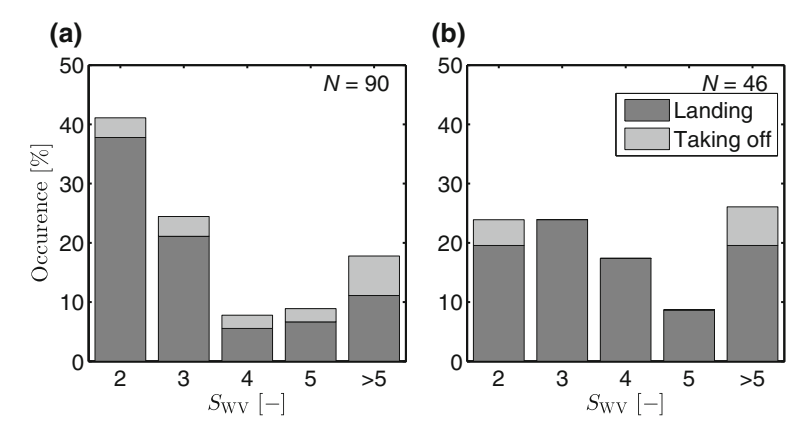


Fig. 6 Histogram of occurrence (in %) of wake vortex intensities for aircraft with wake turbulence category of a medium and $\bf b$ heavy, where 2 on the *x axis* stands for a S_{WV} in between 1 and 2, 3 for a S_{WV} in between 2 and 3, and so on

also apparent from the higher number of wake vortices detected when $\overline{U_\perp} < 0$ than when $\overline{U_\perp} > 0$ (as a percentage of the total detectable 50 % compared with 12 %, respectively). Therefore, in order to increase the detectability of wake vortices for $\overline{U_\perp} > 0$ and for aircraft taking off, a scintillometer would also need to be placed at the other side of the runway (in this case, west).

In Table 1 we note a difference between the percentage of wake vortices detected for aircraft with a medium and heavy wake turbulence category. For both aircraft landings and take offs, there is a clearly higher detectability of the wake vortices created by aircraft with wake turbulence category of heavy (76 and 27 %) compared with wake turbulence category of medium (38 and 14 %). This seems to imply that either wake vortices created by aircraft with a wake turbulence category of medium decay faster than those created by an aircraft with a wake turbulence category of heavy or the wake vortices created by an aircraft with wake turbulence category of medium are weaker.

To investigate the capability of the scintillometer to give a measure of the strength of the wake vortices ($S_{\rm WV}$), Fig. 6 shows the occurrence of different $S_{\rm WV}$ values for aircraft with wake vortex class of medium (Fig. 6a) and heavy (Fig. 6b). For aircraft with wake turbulence category of medium, $S_{\rm WV}$ in between 1 and 2 occurs most often (41 %), while for wake turbulence category of heavy, $S_{\rm WV}$ greater than 6 occurs most often (26 %). The strength of the wake vortices is not influenced by U_{\perp} (not shown), nor by whether an aircraft is landing or taking off. From Fig. 6 we conclude that the scintillometer indeed measures stronger wake vortices when created by an aircraft with wake turbulence category of heavy.

Besides the strength of a wake vortex, the scintillometer can also give a measure of the size of a wake vortex, which is expressed as the time the wake vortex signature is present in the scintillometer signal (see Fig. 7). There is no clear visible difference for wake vortices created by aircraft with a wake turbulence category of medium and heavy. For both categories the wake vortices are mostly present in the scintillometer signals for between 25 and 75 s. However, some wake vortices are present in the scintillometer signal for up to 125 s. Figure 7a indicates that the wake vortex signature is present in the scintillometer signal for longer when $|U_{\perp}|$ is weak (< 1 m s⁻¹).

Figure 8 depicts the separation time between an aircraft landing or taking off and the scintillometer detecting the corresponding wake vortex for different U_{\perp} values. This confirms



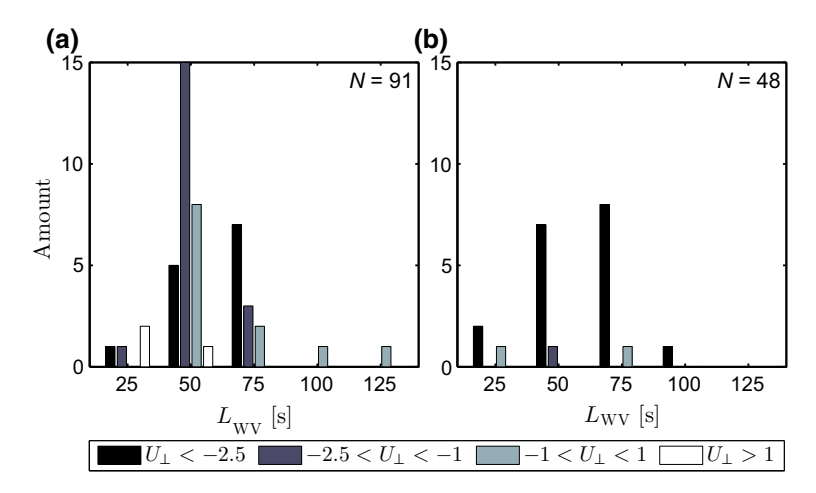


Fig. 7 Bar plots of number of wake vortices of different lengths for aircraft with wake turbulence category of a medium and **b** heavy, where 25 on the x axis stands for a WV_{Length} in between 0 and 25 s, 50 for a WV_{Length} between 25 and 50 s, and so on. The histograms are Color-coded according to U_{\perp}

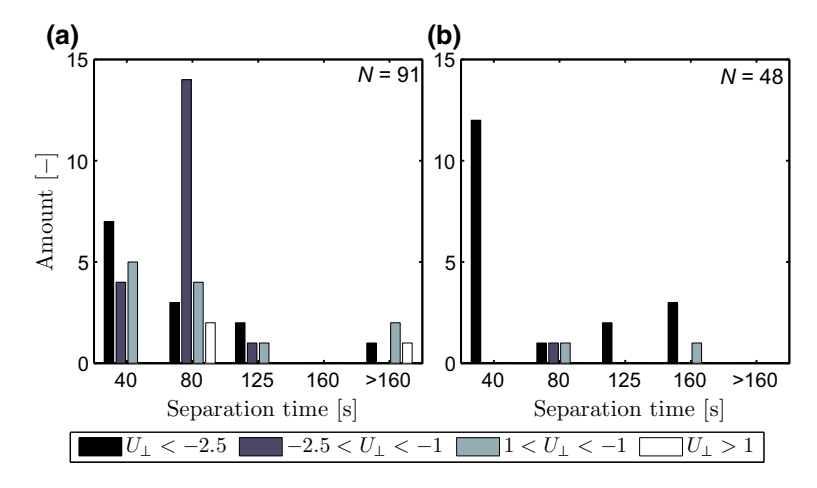


Fig. 8 Bar plots of the time between an aircraft landing or taking off and the scintillometer picking up the wake vortex of the aircraft with a wake turbulence category of $\bf a$ medium and $\bf b$ heavy. On the x axis, 40 stands for a separation time in between 0 and 40 s, 80 for a separation time in between 40 and 80 s, and so on. The histograms are colour-coded according to U_{\perp}

that wake vortices leave the runway with different time scales. Most wake vortices are detected between 0 and 80 s after the aircraft lands or takes off. The figure illustrates again that the wake vortices are transported by the wind; the more negative U_{\perp} (darker colours in Fig. 8), the faster the wake vortices are detected. The aircraft with a wake turbulence category of heavy are in general detected rapidly with often (25 %) only 0 to 40 s in between the aircraft landing or taking off and the detection. For aircraft with a wake turbulence category of medium, separation times between 40 and 80 s occur most often (25 %). From Figs. 7 and 8 we can conclude that taking a set separation distance between aircraft landing and taking off is in reality not necessary, and unnecessarily limits airport capacity. Thus, during stable



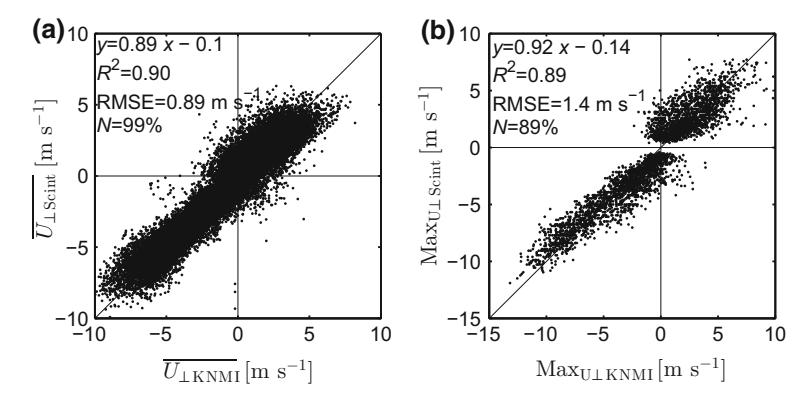


Fig. 9 a Scatterplot of the 10-min average of U_{\perp} measured by the scintillometer $(\overline{U_{\perp}\text{Scint}})$ and KNMI $(\overline{U_{\perp}\text{KNMI}})$. **b** Scatterplot of the maximum U_{\perp} measured by the scintillometer $(\overline{\text{Max}}_{U\perp \text{Scint}})$ and KNMI $(\overline{\text{Max}}_{U\perp \text{KNMI}})$. For both plots the corresponding regression statistics are plotted on the left-hand side and the black line indicates a one-to-one relation

conditions, a scintillometer can detect when a wake vortex has left the runway, leading to an increase of airport capacity.

5.2 Crosswind

The crosswind was measured by the scintillometer over a 3-s time window, while KNMI data were saved every 12 s (see Sect. 4.1). Note that the clocks of the scintillometer and KNMI measurements were not synchronised. Furthermore, the measurement location and height of the scintillometer and KNMI wind data are not the same (see Sect. 4.1). Therefore, the comparison between U_{\perp} measured by the scintillometer (transposed to measurement height of 10 m, see Sect. 4.2) and KNMI is performed over 1-min averages. This comparison is plotted in Fig. 9a. The agreement between the two measurement devices is highly satisfactory. We observe a linear regression slope of 0.89 and a low amount of scatter ($R^2 = 0.90$), leading to an RMSE of 0.89 m s⁻¹. Concluding, the scintillometer is capable of obtaining U_{\perp} correctly near an airport runway over a 3-s time window.

An important parameter in aviation is the maximum U_{\perp} value over the last 10 min $(\text{Max}_{U\perp})$. The results of $\text{Max}_{U\perp}$ are plotted in Fig. 9b. There is a good correlation between the scintillometer $\text{Max}_{U\perp}$ measurements and KNMI $\text{Max}_{U\perp}$ measurements, albeit with more scatter between the two $(R^2=0.89)$ than for U_{\perp} . However, this slightly higher scatter is expected since $\text{Max}_{U\perp}$ corresponds to a 3-s U_{\perp} value. These 3-s values can more easily differ from one another given the different measurement locations and measurement heights of the devices.

5.3 Visibility

Before going into detail about the calibration of $I_{\rm T}$, we first look at Fig. 10a, which shows the normalised scintillation signal against MOR measured by the visibility sensor. From this figure it is apparent that there is a sharp drop in $\overline{I_{\rm R*}}$ when MOR is below 10 km. However, for the early morning hours (in between 0500 and 0700 UTC), there are events where the visibility is above 10 km while $\overline{I_{\rm R*}}$ is below $\frac{2}{3}$ of $I_{\rm R,max}$ (corresponding to a value of 10,000). These events are probably caused by water droplets on the apertures of the scintillometer due to dew, which lowers the scintillometer signal. Therefore, cases in between 0500 and 0700



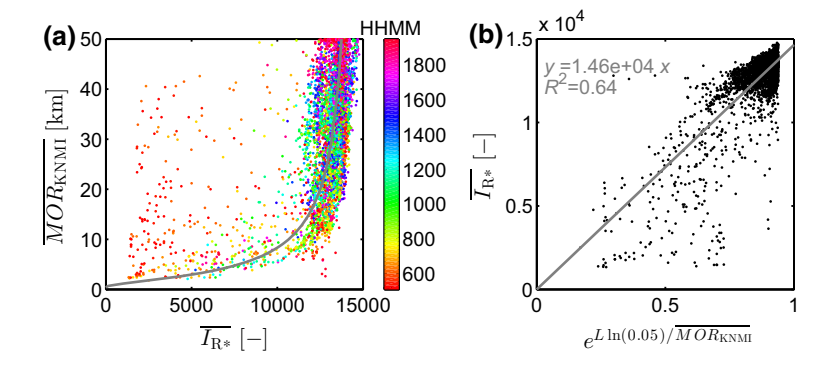


Fig. 10 a Plot of MOR measured by the visibility sensor (MOR_{KNMI}) against $\overline{I_{R*}}$ colour-coded with time given by hour minute (HHMM) HHMM. The *grey line* indicates the values of MOR obtained from $\overline{I_{R*}}$ when using Eq. 5 and I_T from the right figure, where the *grey solid line* indicates MOR calculated from $\overline{I_{R*}}$. **b** Plot of $\overline{I_R}$ against $e^{-L \ln(0.05)/MOR}$, with the regression equation and R^2 with a fit through the origin given in *grey*

UTC where $\overline{I_{R*}} < \frac{2}{3}I_{R,max}$ and MOR > 10 km were excluded from the rest of the visibility analysis.

The calibration of $I_{\rm T}$ is shown in Fig. 10b, where $\overline{I_{\rm R*}}$ is plotted against $e^{-L\ln(0.05)/MOR}$. According to Eqs. 2 and 4, these two quantities should have a linear relation, where the regression slope gives $I_{\rm T}$. There is indeed a linear relationship through the origin visible in Fig. 10b. However, the scatter is reasonably large with an R^2 value of 0.64. This scatter can be caused due to the different measurement locations of the scintillometer and the visibility sensor (see Fig. 2). The regression slope of 1.46×10^4 given in Fig. 10b is in fact the value of $I_{\rm T}$. In Fig. 10a, the grey line indicates the values of MOR calculated with Eq. 5 given the value of $\overline{I_{\rm R*}}$ and using $I_{\rm T}=1.46 \times 10^4$. Given the measurements of $\overline{MOR_{\rm KNMI}}$, there is indeed good correspondence with the MOR calculated from the scintillometer measurements $\overline{(MOR_{\rm Scint})}$ for the different values of $\overline{I_{\rm R*}}$.

Figure 11 shows MOR measured by the visibility sensor (MOR_{KNMI}) and scintillometer (MOR_{Scint}) over the measurement period. From Fig. 11a we note that there is a lot of

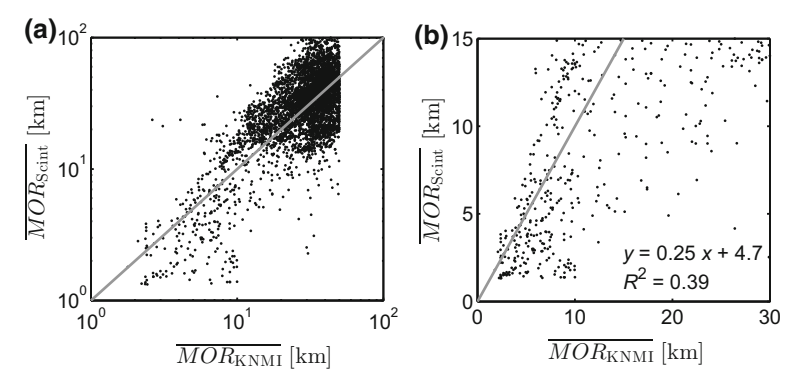


Fig. 11 MOR measured by the visibility sensor $(\overline{MOR_{\text{KNMI}}})$ and the scintillometer $(\overline{MOR_{\text{Scint}}})$ for **a** all values on logarithmic axes, and **b** zoomed into a $\overline{MOR_{\text{Scint}}}$ within 0 and 30 km on normal scale, including the regression statistics. The *grey lines* indicate a one-to-one relation



scatter between $\overline{MOR_{Scint}}$ and $\overline{MOR_{KNMI}}$ for values of $\overline{MOR_{Scint}}$ above 15 km. Therefore, Fig. 11b shows values of $\overline{MOR_{Scint}}$ in between 0 and 15 km of $\overline{MOR_{Scint}}$. Also for these low MOR values, there is a high amount of scatter between that measured by KNMI and by the scintillometer ($R^2 = 0.39$). Besides the scatter, the fit of $\overline{MOR_{Scint}}$ with $\overline{MOR_{KNMI}}$ is also poor, with a regression slope of only 0.25. As discussed above, some of this scatter can be caused by the different measurement locations of the two devices. Thus, it seems that the scintillometer has problems to quantify MOR correctly. However, the scintillometer is able to identify when the visibility drops below 10 km.

6 Conclusions

We investigate the use of a scintillometer installed alongside a runway at Schiphol airport to detect wake vortices, crosswind and visibility. We conclude that, during the night, when the turbulence intensity in the atmosphere is low, a scintillometer is able to detect the presence of a wake vortex in its path, by an increase in $\sigma_{\ln I}^2$. However, during the day, the scintillation signal, and therefore $\sigma_{\ln I}^2$, are dominated by the background atmospheric turbulence, making it impossible to detect wake vortices from the scintillation signal. Besides detecting the presence of a wake vortex, we also develop an algorithm to determine how strong a wake vortex is. The algorithm performs satisfactorily, for aircraft with a heavy wake turbulence category more often producing high values of S_{WV} (>6) than for those with a wake turbulence category of medium. For the present scintillometer set-up, the wake vortices created by aircraft that landed are more often detected than those created by aircraft that took off. This is probably due to the different wind regime during landing and taking off (mostly southsouth-west during landing and north-north-east during take off). In order to increase the detectability of wake vortices created by aircraft that take off, another scintillometer needs to be set up at the other side of the runway (in this case at the west side). It is also possible that the different evolution of wake vortices created by aircraft which are landing and taking off (fully developed versus in the process of development) result in differences in detectability. Further, the detectability can also be increased by placing the scintillometer as close as possible to the runway. We detected 39 wake vortices even though no aircraft landed or took off in the previous 3.5 min (i.e. false wake vortex detections), which are probably caused by an increase of $\sigma_{\ln I}^2$ related to the background atmospheric turbulence. The results of the detection of the wake vortices show that the time it takes for a wake vortex to be transported away from the runway is variable (mostly in between 40 and 125 s), making a set separation time unnecessary.

Our results show that a scintillometer is able to obtain correct values of the crosswind also near an airport runway over a 3-s time window. However, in order to achieve correct crosswind estimations, a filter on outliers has to be applied. We highlight that after the filtering procedure it is still possible to obtain the maximum crosswind over a 10-min time window, which is an important quantity for aviation.

For visibility we find that it is difficult to obtain the exact value of *MOR* from the signal intensity of the scintillometer. Albeit with some scatter, the scintillometer is able to obtain the visibility up to 10 km. In order to achieve these results some issues have to be addressed. First, alignment issues can result in a decrease in the scintillometer signal, which can be misinterpreted as low visibility conditions. Therefore, in this study the signal is adjusted for alignment issues. Second, dew on the apertures of the scintillometer can result in a lowering of the scintillation signal. Thus in order to measure visibility it is recommendable to use



scintillometers that heat the aperture, to minimise the influence of dew on the scintillation signal.

Acknowledgments The authors would like to thank Kees van den Dries and Jan-Willem Schoonderwoerd for their help in the field, Ben Wichers Schreur for supplying KNMI data and Evert Westerveld for supplying the wake turbulence category data. Further, the authors also thank Marco Ponsen, Jan-Otto Haanstra, Peter van den Brink, Martin Dikker, Jan Sondij, Henk Klein Baltink, Paul van Es, Jan Meijer, Frits van Peppel, Rob Poelsma and Jan Elbers for making it possible to carry out this experiment at Schiphol airport. Daniëlle van Dinther and Oscar Hartogensis were supported by the Knowledge for Climate project Theme 6 entitled "High Quality Climate Projections" (KVK-HS2).

Open Access This article is distributed under the terms of the Creative Commons Attribution 4.0 International License (http://creativecommons.org/licenses/by/4.0/), which permits unrestricted use, distribution, and reproduction in any medium, provided you give appropriate credit to the original author(s) and the source, provide a link to the Creative Commons license, and indicate if changes were made.

References

Andreas EL (ed) (1990) Selected papers on turbulence in a refractive medium, vol 25. SPIE Optical Engineering Press, Bellingham

De Bruin HAR (2002) Introduction: renaissance of scintillometry. Boundary-Layer Meteorol 105(1):1-4

Earnshaw KB, Wang TI, Lawrence RS, Greunke RG (1978) A feasibility study of identifying weather by laser forward scattering. J Appl Meteorol 17(10):1476–1481

Gerz T, Holzäpfel F, Darracq D (2002) Commercial aircraft wake vortices. Prog Aerosp Sci 38:181-208

Gerz T, Holzäpfel F, Bryant W, Köpp F, Frech M, Tafferner A, Winckelmans G (2005) Research towards a wake-vortex advisory system for optimal aircraft spacing. C R Phys 6:501–523

Godwin KS, De Wekker SFJ, Emmitt GD (2012) Retrieving winds in the surface layer over land using an airborne Doppler lidar. J Atmos Ocean Technol 29(4):487–499

Green AE, Astill MS, McAneney KJ, Nieveen JP (2001) Path-averaged surface fluxes determined from infrared and microwave scintillometers. Agric For Meteorol 109(3):233–247

Hallock JN, Osgood SP (2003) Wake vortex effects on parallel runway operations. Amer Inst Aeronaut Astronaut 379:1–11

Harris M, Young RI, Köpp F, Dolfi A, Cariou JP (2002) Wake vortex detection and monitoring. Aerosp Sci Technol 6(5):325–331

Holzäpfel F, Steen M (2007) Aircraft wake-vortex evolution in ground proximity: analysis and parameterization. Am Inst Aeronaut Astronaut 45(1):218–227

Holzäpfel F, Hofbauer T, Darracq D, Moet H, Garnier F, Cago CF (2003) Analysis of wake vortex decay mechanisms in the atmosphere. Aerosp Sci Technol 7:263–275

Kolmogorov AN (1941) The local structure of turbulence in an incompressible viscous fluid for very large Reynolds numbers. Dokl Akad Nauk 30:299–303

Koschmieder H (1924) Theorie der horizontalen Sichtweite. Beitr Phys Freie Atmos 12:171-181

Krasny R (1987) Computation of vortex sheet roll-up in the Trefftz plane. J Fluid Mech 184:123-155

Lawrence RS, Ochs GR, Clifford SF (1972) Use of scintillations to measure average wind across a light beam. Appl Opt 11(2):239–243

Meijninger WML, de Bruin HAR (2000) The sensible heat fluxes over irrigated areas in western Turkey determined with a large aperture scintillometer. J Hydrol 229:42–49

Meulen JP van der (1998) Wake vortex induced wind measurements at airfields: A simple algorithm to reduce the vortex impact. Instruments and Observing Methods Reports WMO/TD No. 7)

Poggio LP, Furger M, Prévôt AH, Graber WK, Andreas EL (2000) Scintillometer wind measurements over complex terrain. J Atmos Ocean Technol 17(1):17–26

Robins RE, Delisit DP (1993) Potential hazard of aircraft wake vortices in ground effect with crosswind. J Aircr 30(2):201–206

Robinson PJ (1989) The influence of weather on flight operations at the Atlanta Hartsfield International Airport. Weather Forecast 4:461–468

Tatarskii VI (1961) Wave propagation in a turbulent medium. McGraw-Hill, New York, 285 pp

van Dinther D, Hartogensis OK (2014) Using the time-lag-correlation function of dual-aperture-scintillometer measurements to obtain the crosswind. J Atmos Ocean Technol 31(1):62–78



- van Dinther D, Hartogensis OK, Moene AF (2013) Crosswinds from a single-aperture scintillometer using spectral techniques. J Atmos Ocean Technol 30(1):3–21
- van der Velde IR, Steeneveld GJ, Wichers Schreur BGJ, Holtslag AAM (2010) Modeling and forecasting the onset and duration of severe radiation fog under frost conditions. Mon Weather Rev 138(11):4237–4253
- Vogt H (1968) Visibility measurement using backscattered light. J Atmos Sci 25:912–918
- Wang TI, Ochs GR, Lawrence RS (1981) Wind measurements by the temporal cross-correlation of the optical scintillations. Appl Opt 20(23):4073–81
- Werner C, Streicher J, Leike I, Münkel C (2005) Visibility and cloud lidar. In: Weitkamp C (ed) Lidar rangeresolved optical remote sensing of the atmosphere, vol 6. Springer, New York, pp 164–186
- Wheelon AD (2006) Electromagnetic scinillation. II Weak scattering. Cambridge University Press, Cambridge, UK, 464 pp



